HHS Public Access

Author manuscript

AJR Am J Roentgenol. Author manuscript; available in PMC 2019 May 25.

Published in final edited form as:

AJR Am J Roentgenol. 2016 November ; 207(5): 1159–1166. doi:10.2214/AJR.15.15957.

Kinetic Analysis of Benign and Malignant Breast Lesions With Ultrafast Dynamic Contrast-Enhanced MRI: Comparison With Standard Kinetic Assessment

Hiroyuki Abe[1], **Naoko Mori**[2], **Keiko Tsuchiya**[1], **David V. Schacht**[1], **Federico D. Pineda**[1], **Yulei Jiang**[1], and **Gregory S. Karczmar**[1]

[1]Department of Radiology, The University of Chicago, 5841 S Maryland Ave, MC2026, Chicago, IL 60637

[2]Department of Diagnostic Radiology, Tohoku University Graduate School of Medicine, Sendai, Japan

Abstract

OBJECTIVE.—The purposes of this study were to evaluate diagnostic parameters measured with ultrafast MRI acquisition and with standard acquisition and to compare diagnostic utility for differentiating benign from malignant lesions.

MATERIALS AND METHODS.—Ultrafast acquisition is a high-temporal-resolution (7 seconds) imaging technique for obtaining 3D whole-breast images. The dynamic contrast-enhanced 3-T MRI protocol consists of an unenhanced standard and an ultrafast acquisition that includes eight contrast-enhanced ultrafast images and four standard images. Retrospective assessment was performed for 60 patients with 33 malignant and 29 benign lesions. A computer-aided detection system was used to obtain initial enhancement rate and signal enhancement ratio (SER) by means of identification of a voxel showing the highest signal intensity in the first phase of standard imaging. From the same voxel, the enhancement rate at each time point of the ultrafast acquisition and the AUC of the kinetic curve from zero to each time point of ultrafast imaging were obtained.

RESULTS.—There was a statistically significant difference between benign and malignant lesions in enhancement rate and kinetic AUC for ultrafast imaging and also in initial enhancement rate and SER for standard imaging. ROC analysis showed no significant differences between enhancement rate in ultrafast imaging and SER or initial enhancement rate in standard imaging.

CONCLUSION.—Ultrafast imaging is useful for discriminating benign from malignant lesions. The differential utility of ultrafast imaging is comparable to that of standard kinetic assessment in a shorter study time.

Keywords

breast; cancer; kinetics; MRI; ultrafast

Address correspondence to H. Abe (habe@radiology.bsd.uchicago.edu).

Breast MRI is well established in clinical practice as having high sensitivity and reasonable specificity in the detection of breast cancer [1–7]. Standard breast MRI techniques entail dynamic contrast-enhanced (DCE) imaging with a T1-weighted sequence performed before and after IV injection of a gadolinium-based contrast agent. In clinical practice, benign and malignant lesions are differentiated by means of morphologic evaluation of the lesion and assessment of the kinetic curve, which shows signal enhancement in relation to time after contrast injection. For the kinetic curve assessment, radiologists qualitatively measure the curve shape according to the BI-RADS lexicon [8]. Previous reports [9, 10] have shown that a curve showing fast initial enhancement and late washout would suggest malignancy, whereas slow initial enhancement and late persistent washout would suggest benignity. For standard kinetic assessment, a delayed image is required so that the late time point can be obtained for kinetic analysis, which results in a long acquisition time.

Results of previous studies [11–16] have suggested that parameters measured in the early phase of contrast enhancement, such as timing of enhancement, initial AUC, and initial slope of enhancement, are useful for differentiation of benign and malignant lesions. In those studies, these values were calculated from standard DCE-MR images, high-temporal-resolution images of selected slices, or high-temporal-resolution images evaluated with view-sharing methods (e.g., time-resolved angiography with interleaved stochastic trajectories [TWIST] or time-resolved imaging of contrast kinetics [TRICKS]) or compressed sensing [17–21]. With standard DCE-MRI, temporal resolution is typically greater than 60 seconds. As a result, important kinetic information in the early phase is obscured. The view-sharing and compressed-sensing methods can cause artifacts, which decrease the reliability of quantitative analysis [22].

We have developed an MRI protocol, which we call ultrafast imaging, whereby whole-breast 3D images are acquired with very high temporal resolution (7 seconds) by use of higher than usual sensitivity-encoded (SENSE) acceleration factors and lower than usual spatial resolution. Because whole-breast 3D data are acquired at multiple time points immediately after contrast injection, more realistic diagnostic parameters from the kinetic curves can be obtained. In our clinical practice, we perform the ultrafast acquisition during the early phase of contrast enhancement for approximately 1 minute. It is followed by a standard high-resolution contrast-enhanced T1-weighted acquisition. This allows sampling of the kinetics of contrast uptake at high temporal resolution immediately after contrast injection.

In this study, we compared the diagnostic parameters measured on the ultrafast images with those from standard images and evaluated the diagnostic accuracy of these two approaches in terms of differentiation of benign and malignant lesions.

Materials and Methods

This retrospective study was HIPAA compliant and received institutional review board approval with a waiver of the requirement for written informed consent.

Patients

We retrospectively reviewed breast MRI studies obtained at out institution between January 1, 2015, and September 30, 2015. Among 201 patients who underwent 3-T breast MRI, 94 consecutively registered patients had biopsy-proven benign or malignant lesions or clinically confirmed benign lesions. The following were excluded: 11 patients imaged with a different MRI protocol, 20 patients who underwent neoadjuvant chemotherapy, and three patients whose MRI studies had technical errors. Consequently, a total of 60 patients with 33 malignant and 29 benign lesions participated in this retrospective study. Two patients had two lesions: one patient had a benign lesion in one breast and another benign lesion in the contralateral breast, and the other patient had a malignant lesion in one breast and a benign lesion in the contralateral breast. The malignant lesions were 28 infiltrating ductal carcinomas, two ductal carcinomas in situ, one infiltrating lobular carcinoma, one metaplastic carcinoma, and one pleomorphic lobular carcinoma in situ. The benign lesions were 12 fibroadenomas; four usual ductal hyperplasia; four chronic inflammation; three papillomas; and one each of adenosis, apocrine metaplasia, fibrotic stroma, lactation-like changes, atrophic changes, and inflamed duct. Pathologic proof was obtained by percutaneous core needle biopsy for all but three benign lesions (all fibroadenomas), which were clinically diagnosed with follow-up imaging using either mammography or ultrasound lasting more than 2 years. Patient age, menopausal status, tumor size, and tumor MRI features are summarized in Table 1.

MRI Protocols

DCE-MRI was performed with an Achieva 3 T-TX system (Philips Healthcare) and 16-channel bilateral breast coils (MammoTrak, Philips Healthcare). The ultrafast acquisition was a T1-weighted fat-suppressed sequence with an increased SENSE factor, reduced spatial resolution, and very high temporal resolution (7 seconds). The acquisition parameters for ultrafast and standard imaging are summarized in Table 2. The DCE series consisted of one standard and five ultrafast acquisitions before contrast injection and then eight ultrafast and four standard acquisitions after injection of gadobenate dimeglumine (MultiHance, Bracco) at a dose of 0.1 mM/kg and a rate of 2 mL/s followed by a 20-mL saline flush at a rate of 2 mL/s. We obtained five unenhanced images purely for research purposes; the last (5th) unenhanced image was used for the subtraction mask. Acquisition of the ultrafast contrast-enhanced series started 10 seconds after the beginning of contrast injection and ended 66 seconds after the beginning of the injection. The standard acquisition started immediately after completion of the ultrafast acquisition and ended 5 minutes 26 seconds after the beginning of the contrast injection. Figure 1 shows the ultrafast and standard imaging protocols.

Data Analysis

All lesions were evaluated retrospectively with a commercial CAD system (Dynacad, version 2.1.7, Philips Healthcare). The software generated color-coded maps of the standard images that represented changes in signal intensity over time. We used the first contrast-enhanced standard images as the early image and the last (4th) contrast-enhanced standard image as the delayed image. Because peak enhancement of breast lesions is typically

observed 1.5 minutes after contrast injection, the first standard image was the optimal timing to set as the early image [11]. Each voxel was color-coded red (washout pattern), blue (persistent pattern), or green (plateau pattern) based on the change in signal intensity between the early and delayed images according to the BI-RADS lexicon [8]. In addition, the CAD system showed the voxel signal intensity when the user placed a cursor over a voxel. Subtraction images were used to assess the lesions. One radiologist (7 years of experience in breast MRI) manually identified, with the help of the color-coded map, a single voxel within each lesion that had the highest signal intensity on the early image for 41 lesions. Another radiologist (12 years of experience in breast MRI) did the same for the other 21 lesions. From this voxel, the initial enhancement rate and the signal enhancement ratio (SER) were calculated. Initial enhancement rate was defined as S_{early} / S_{pre} and SER as $(S_{early} - S_{unenhanced}) / (S_{delayed} - S_{unenhanced})$, where S is the signal intensity of the manually identified voxel on the unenhanced, early, and delayed phase contrast-enhanced standard images.

Initial enhancement rate and SER are commonly used to quantify the early and delayed components of the standard kinetic curve [23, 24]. Initial enhancement rate is reported to be an effective parameter for differentiating malignant from benign breast lesions [25–27]. It represents the initial increase in contrast enhancement in the kinetic assessment for BI-RADS. An intensity increase < 50% is classified as slow, 50–100% as medium, and > 100% as fast enhancement. SER indicates the kinetic curve shape that represents the delayed phase in BI-RADS assessment. Persistent is more than 10% of initial enhancement, washout is less than 10% of initial enhancement, and plateau is between the two. Therefore, SER < 0.91 (100/110) indicates the persistent enhancement pattern, SER > 1.11 (100/90) indicates the washout enhancement pattern, and $0.91 \leq SER \leq 1.11$ indicates the plateau enhancement pattern. Initial enhancement rate and SER were used in this study as the reference standards for evaluation of the ultrafast images.

The manually identified voxel of the highest enhancement on the early contrast-enhanced standard image was then identified on the ultrafast contrast-enhanced images. Enhancement rate at each of the ultrafast time points was calculated from this voxel (Fig. 2), and the AUC of the kinetic curve for the ultrafast images was obtained with a simple geometric calculation (Fig. 3). To compensate for differences in time of arrival of contrast medium, time points on the ultrafast images were relative to the initial contrast enhancement in the descending aorta at the level of the nipple. We referred to the time point when the aorta began to become enhanced as C1 and to subsequent time points as C2, C3, and so on (Fig. 4). C1 was identified when the signal intensity within an ROI in the aorta became more than twice the average signal intensity of the five unenhanced images within the same ROI. The enhancement rates at C1, C2, and so on were used in this study for evaluation of the ultrafast images for differentiation between malignant and benign lesions. To assess interobserver variability, a third radiologist (4 years of experience in breast MRI) repeated these analyses with the same procedure.

Statistical Analysis

The Mann-Whitney *U* test was used for comparing patient age, tumor size, enhancement rate, kinetic AUC, initial enhancement rate, and SER between malignant and benign lesions. The chisquare test was used for comparing menopausal status, and the Fisher exact test for comparing MRI features of mass as opposed to nonmass lesions. ROC analysis and ROC AUC were used to evaluate the diagnostic merit of all parameters. Maximum likelihood binormal ROC curves were estimated, and the AUCs were compared between two ROC curves by use of the CLABROC algorithm [25, 26]. Interclass correlation coefficient (ICC) was used to evaluate interobserver variability with the following qualitative interpretation: a value of 1.0 was considered perfect agreement; 0.81–0.99, almost perfect agreement; 0.61–0.80, substantial agreement; 0.41–0.60, moderate agreement; 0.21–0.40, fair agreement; and 0.20 or less, slight agreement [27]. The optimal threshold for discrimination between malignant and benign lesions was chosen at the highest possible sensitivity and specificity (maximum Youden index defined as sensitivity plus specificity minus 1) on the ROC curve [28]. Statistical analyses were performed with JMP Pro 11 software (SAS Institute). A value of $p < 0.05$ was considered statistically significant; after Bon-ferroni correction of 21 multiple comparisons, the critical value became $\alpha = 0.0024$ (0.05/21).

Results

In the comparison of malignant and benign lesions, there were no statistically significant differences in patient age, menopausal status, or mass as opposed to nonmass MRI features, but there was a significant difference in tumor size (Table 1). There were statistically significant differences in SER ($p = 0.0001$) and initial enhancement rate ($p = 0.0014$) between malignant and benign lesions. The AUC value (± standard error) for differentiation between malignant and benign lesions for initial enhancement rate was 0.72 ± 0.06 and for SER was 0.88 ± 0.04 (Table 3).

For the ultrafast images, the earliest contrast enhancement of the aorta was seen on the first contrast-enhanced ultrafast image of 31 patients, at the second contrast-enhanced ultrafast image of 28 patients, and at the third contrast-enhanced ultrafast image of one patient among the total of 60 patients. As a result, not all patients had C7 and C8 images because we defined C1 as the ultrafast time point of the earliest contrast enhancement in the aorta Thus, for all patients, we evaluated enhancement rate and kinetic AUC at C1–C6 but not at C7 or C8.

There were statistically significant differences between malignant and benign lesions in enhancement rate at C2–C6 ($p \leq 0.0001$) and in kinetic AUC at C2-C6 ($p \leq 0.0001$) (Table 4). The AUC for enhancement rate was greater than 0.80 at C2–C5, and it was highest at C2 (0.87 ± 0.04). The AUC value for kinetic AUC was greater than 0.85 at C2–C5, and it was highest at C3 (0.89 ± 0.04) (Table 4). The AUC for enhancement rate at C2 was not statistically significantly different from that for SER ($p = 0.95$), but the AUC of enhancement rate at C2 ($p = 0.004$) was close to being significantly greater than the AUC of initial enhancement rate (Fig. 5). With use of 116% as the cutoff enhancement rate at C2, performance according to an analysis of the Youden index would have been as follows:

sensitivity, 85%; specificity, 79%; positive predictive value (PPV), 82%; negative predictive value (NPV), 82%.

The ICC values for assessment of interobserver variability are shown in Tables 3 and 4. The ICC exceeded 0.87 for enhancement rate and kinetic AUC of the ultrafast images and for initial enhancement rate of the standard image, indicating almost perfect agreement. The ICC was 0.78 for SER of the standard image, indicating substantial agreement.

Discussion

Kinetic information is considered useful for differentiation of benign and malignant lesions on breast MRI studies. However, the limitations of obtaining standard kinetic information include misregistration artifact due to long acquisition time and obtaining images that may not be useful for clinical interpretation. Misregistration artifact caused by patient motion is encountered frequently on subtraction images and tends to have a greater effect with longer acquisition time. Misregistration artifact jeopardizes kinetic assessment, affects the quality of subtraction images, and can even result in uninterpretable studies [29]. Although multiple phase images are obtained after contrast injection, most of the information useful for clinical interpretation is obtained in the early phase. Because background parenchymal enhancement (BPE) becomes more evident and obscures true lesions in the later phases, images from late phases may not be useful. Thus, it is desirable to reduce acquisition time and alleviate problems related to motion on delayed images. In addition, acquiring delayed phase images increases time in the MRI suite, which contributes to the high cost of breast MRI.

Our study showed no significant difference in the AUCs of enhancement rate at C2 and SER ($p = 0.95$) and an apparent larger AUC for enhancement rate at C2 than for initial enhancement rate ($p = 0.004$). These results suggest that kinetic assessment of ultrafast imaging may be comparable to that of standard imaging. In this study, sensitivity (85%), specificity (79%), PPV (82%), and NPV (82%) of the enhancement rate at C2 were obtained from the ROC curve based on the Youden index. Previous studies [11, 12, 30, 31] showed the diagnostic performance of kinetic assessment was sensitivity of 67–97%, specificity of 18–73%, PPV of 72–88%, and NPV of 46–82%. Our results appear to be comparable to the previously reported results. In addition, our results showed apparently higher specificity than did the earlier studies. If our results are adjusted for a lower specificity value to 50%, which is the average specificity of the four previous studies, our sensitivity, PPV, and NPV are 96%, 71% and 90%. Thus, we believe that our results for ultrafast imaging are comparable to the previous results for standard kinetic assessment. Although kinetic assessment performs well in differentiation of benign and malignant lesions, the final assessment should still be based on the combination of morphologic and kinetic assessment. We agree with the BI-RADS guideline that assessment of breast lesions not be based solely on kinetic features. Therefore, a single standard image should be added after the contrast-enhanced ultrafast acquisition, and morphologic assessment should be performed on the high-resolution standard image because the spatial resolution of ultrafast images is lower than that of standard images. Nevertheless, delayed images will not be needed, resulting in shorter imaging time.

In this study, we performed kinetic assessment of both standard and ultrafast images using a commercially available CAD system. Because, like standard imaging, ultrafast imaging consists of multiphase unenhanced and contrast-enhanced series, commercially available CAD systems can be used to view subtraction images and obtain kinetic curves from the ultrafast images. With minor modifications to the CAD system, one can also produce color-coded maps from the ultrafast images based on the enhancement rate and kinetic AUC, which may be useful for clinical interpretation.

Although we did not specifically compare BPE between the ultrafast and standard images, we expect BPE to be less on ultrafast images because these images are obtained earlier during contrast enhancement because normal parenchyma becomes enhanced more slowly than lesions do [32]. It has been reported [33] that BPE negatively affects the detection, diagnosis, and staging of breast cancer. The contrast-enhanced ultrafast images yield multiple 3D datasets of the entire breast in the same time that standard contrast-enhanced imaging yields only one 3D dataset after contrast injection. Ultrafast imaging increases the likelihood of obtaining high contrast ratios between a tumor and BPE.

Pharmacokinetic compartment modeling of DCE-MRI has been investigated extensively as a potentially robust approach to deriving standardized physiologic parameters [34]. However, this technique is difficult to implement in daily clinical practice. It requires precise measurement of the arterial input function and unenhanced T1 value, both of which are known to be subject to considerable error without standardized methods of measurement [35]. Although the native T1 and arterial input function can be estimated, the approximation methods are not straightforward or applicable to daily clinical practice [12, 36–39]. In this study, our results obtained with a conventional method of acquiring ultrafast images yielded parameter values more accurate than those estimated from standard images and results comparable to those from standard images for differentiating benign from malignant lesions. These results suggest that ultrafast imaging can be implemented easily in routine clinical practice as an effective technique to complement and improve standard imaging. Because we did not use special hardware or special software to perform ultrafast imaging, this acquisition can be performed with any 3-T MRI system.

The American College of Radiology (ACR) accreditation of breast MRI requires unenhanced, early contrast-enhanced (within 4 minutes of contrast injection), and delayed contrast-enhanced T1-weighted series [40]. Our ultrafast acquisition takes less than 1 minute, and the standard acquisition can follow without time delay. It takes 131 seconds to obtain the contrast-enhanced ultrafast images and the first standard image after contrast injection, and even the second contrast-enhanced standard image can be obtained within 4 minutes after contrast injection. Therefore, ultrafast imaging can be implemented in standard breast MRI sequences while satisfying the ACR requirement.

One limitation of this study was that for assessment of enhancement rate and kinetic AUC from the ultrafast images, we used the most enhancing voxel within a lesion, which is consistent with kinetic assessment described for BI-RADS [8]. However, it is understood that tumors are heterogeneous, and malignant tumors tend to be more heterogeneous than benign tumors [24, 41]. Thus, one voxel of a tumor may not represent all characteristics of

the tumor. Although the BI-RADS guidelines call for the use of the most suspicious portion of a lesion to assess kinetic information, a volumetric assessment may be preferable and will be tested in the future. A second limitation was the number and types of cases included in this study. The malignant lesions were mostly invasive and rather large, and the benign lesions were small. The malignant lesions were predominantly mass lesions, and there were only a few lesions with nonmass enhancement. The small number of cases is likely a major cause of the lack of statistical significance ($p = 0.004$ compared with the critical value of $\alpha = 0.0024$) between the AUC for the enhancement rate at C2 (AUC, 0.87 ± 0.04) and that for initial enhancement rate (AUC, 0.72 ± 0.06), although the AUC of enhancement rate at C2 was apparently larger than that of initial enhancement rate. A follow-up study with a larger number of cases and a subgroup analysis according to the lesion shape, size, or pathologic features should be performed to evaluate the robustness of our methods. A third limitation was that we used only a 3-T MRI system in this study. Ultrafast acquisition can also be performed with 1.5-T systems, but the temporal resolution is lower, and image quality is reduced in relation to that of 3-T systems. If image quality can be improved, it would be preferable to perform ultrafast imaging with 1.5-T MRI systems because they are more widely available.

Conclusion

Our results show that the kinetic parameters measured with ultrafast imaging are useful for discriminating benign from malignant lesions and that ultrafast imaging is comparable to standard imaging for differentiation between benign and malignant lesions. However, acquisition time and the effects of patient motion may be reduced with ultrafast imaging. Ultrafast imaging can be easily implemented in standard breast MRI protocols, and the kinetic analysis we describe can be performed with widely available commercial software. Therefore, the methods we describe can easily be implemented in community hospitals. Development of specialized methods of data acquisition and analysis based on ultrafast imaging findings may eventually lead to increased diagnostic accuracy.

References

1. Kuhl CK. Mammography, breast ultrasound, and magnetic resonance imaging for surveillance of women at high familial risk for breast cancer. J Clin Oncol 2005; 23:8469–8476 [PubMed: 16293877]
2. Kriege M, Brekelmans CT, Boetes C, et al. Efficacy of MRI and mammography for breast-cancer screening in women with a familial or genetic predisposition. N Engl J Med 2004; 351:427–437 [PubMed: 15282350]
3. Warner E, Plewes DB, Hill KA, et al. Surveillance of BRCA1 and BRCA2 mutation carriers with magnetic resonance imaging, ultrasound, mammography, and clinical breast examination. JAMA 2004; 292:1317–1325 [PubMed: 15367553]
4. Warner E, Messersmith H, Causer P, Eisen A, Shumak R, Plewes D. Systematic review: using magnetic resonance imaging to screen women at high risk for breast cancer. Ann Intern Med 2008; 148:671–679 [PubMed: 18458280]
5. Lehman CD, Blume JD, Weatherall P, et al. Screening women at high risk for breast cancer with mammography and magnetic resonance imaging. Cancer 2005; 103:1898–1905 [PubMed: 15800894]

6. Sardanelli F, Podo F, D'Agnolo G, et al. Multi-center comparative multimodality surveillance of women at genetic-familial high risk for breast cancer (HIBCRIT Study): interim results. Radiology 2007; 242:698–715 [PubMed: 17244718]
7. Saslow D, Boetes C, Burke W, et al. American Cancer Society guidelines for breast screening with MRI as an adjunct to mammography. CA Cancer J Clin 2007; 57:75–89 [PubMed: 17392385]
8. Morris EA, Comstock CE, Lee CH, et al. ACR BI-RADS Magnetic Resonance Imaging. In: D'Orsi CJ, Sickles EA, Mendelson EB, Morris EA, et al. ACR BI-RADS Atlas, Breast Imaging Reporting and Data System. Reston, VA: American College of Radiology, 2013
9. Kuhl CK, Mielcareck P, Klaschik S, et al. Dynamic breast MR imaging: are signal intensity time course data useful for differential diagnosis of enhancing lesions? Radiology 1999; 211:101–110 [PubMed: 10189459]
10. Kuhl CK, Schild HH. Dynamic image interpretation of MRI of the breast. J Magn Reson Imaging 2000; 12:965–974 [PubMed: 11105038]
11. Szabó BK, Aspelin P, Wiberg MK, Boné B. Dynamic MR. imaging of the breast: analysis of kinetic and morphologic diagnostic criteria. Acta Radiol 2003; 44:379–386 [PubMed: 12846687]
12. Jansen SA, Fan X, Karczmar GS, Abe H, Schmidt RA, Newstead GM. Differentiation between benign and malignant breast lesions detected by bilateral dynamic contrast-enhanced MRI: a sensitivity and specificity study. Magn Reson Med 2008; 59:747–754 [PubMed: 18383287]
13. Moate PJ, Dougherty L, Schnall MD, Landis RJ, Boston RC. A modified logistic model to describe gadolinium kinetics in breast tumors. Magn Reson Imaging 2004; 22:467–473 [PubMed: 15120165]
14. Buadu LD, Murakami J, Murayama S, et al. Breast lesions: correlation of contrast medium enhancement patterns on MR images with histopathologic findings and tumor angiogenesis. Radiology 1996; 200:639–649 [PubMed: 8756909]
15. Chung WJ, Kim HS, Kim N, Choi CG, Kim SJ. Recurrent glioblastoma: optimum area under the curve method derived from dynamic contrast-enhanced T1-weighted perfusion MR imaging. Radiology 2013; 269:561–568 [PubMed: 23878286]
16. Boetes C, Barentsz JO, Mus RD, et al. MR characterization of suspicious breast lesions with a gadolinium-enhanced TurboFLASH subtraction technique. Radiology 1994; 193:777–781 [PubMed: 7972823]
17. Ramsay E, Causer P, Hill K, Plewes D. Adaptive bilateral breast MRI using projection reconstruction time-resolved imaging of contrast kinetics. J Magn Reson Imaging 2006; 24:617–624 [PubMed: 16892204]
18. Tudorica LA, Oh KY, Roy N, et al. A feasible high spatiotemporal resolution breast DCE-MRI protocol for clinical settings. Magn Reson Imaging 2012; 30:1257–1267 [PubMed: 22770687]
19. Hargreaves BA, Saranathan M, Sung K, Daniel BL. Accelerated breast MRI with compressed sensing. Eur J Radiol 2012; 81:S54–S55 [PubMed: 23083601]
20. Wang H, Miao Y, Zhou K, et al. Feasibility of high temporal resolution breast DCE-MRI using compressed sensing theory. Med Phys 2010; 37:4971–4981 [PubMed: 20964216]
21. Mann RM, Mus RD, Jan van Zelst MD, Geppert C, Karssemeijer N, Platel B. A novel approach to contrast-enhanced breast magnetic resonance imaging for screening. Invest Radiol 2014; 49:579–585 [PubMed: 24691143]
22. Chenevert TL, Helvie MA, Aisen AM, et al. Dynamic three-dimensional imaging with partial k-space sampling: initial application for gadolinium-enhanced rate characterization of breast lesions. Radiology 1995; 196:135–142 [PubMed: 7784556]
23. Millet I, Curros-Doyon F, Molinari N, et al. Invasive breast carcinoma: influence of prognosis and patient-related factors on kinetic MR imaging characteristics. Radiology 2014; 270:57–66 [PubMed: 24029641]
24. Shimauchi A, Abe H, Schacht DV, et al. Evaluation of kinetic entropy of breast masses initially found on MRI using whole-lesion curve distribution data: comparison with the standard kinetic analysis. Eur Radiol 2015; 25:2470–2478 [PubMed: 25698353]
25. Metz CE, Herman BA, Shen JH. Maximum likelihood estimation of receiver operating characteristic (ROC) curves from continuously-distributed data. Stat Med 1998; 17:1033–1053 [PubMed: 9612889]

26. Metz CE, Wang PL, Kronman HB. A new approach for testing the significance of differences between ROC curves measured from correlated data. In: Deconinck F, ed. Information processing in medical imaging The Hague, The Netherlands: Nijhoff, 1984:432–445
27. Landis JR, Koch GG. The measurement of observer agreement for categorical data. Biometrics 1977; 33:159–174 [PubMed: 843571]
28. Youden WJ. Index for rating diagnostic tests. Cancer 1950; 3:32–35 [PubMed: 15405679]
29. Morris EA. Breast cancer imaging with MRI. Radiol Clin North Am 2002; 40:443–466 [PubMed: 12117186]
30. Newell D, Nie K, Chen JH, et al. Selection of diagnostic features on breast MRI to differentiate between malignant and benign lesions using computer-aided diagnosis: differences in lesions presenting as mass and non-mass-like enhance-ment. Eur Radiol 2010; 20:771–781 [PubMed: 19789878]
31. Leinsinger G, Schlossbauer T, Scherr M, Lange O, Reiser M, Wismüller A. Cluster analysis of signal-intensity time course in dynamic breast MRI: does unsupervised vector quantization help to evaluate small mammographic lesions? Eur Radiol 2006; 16:1138–1146 [PubMed: 16418862]
32. Jansen SA, Fan X, Medved M, et al. Characterizing early contrast uptake of ductal carcinoma in situ with high temporal resolution dynamic contrast-enhanced MRI of the breast: a pilot study. Phys Med Biol 2010; 55:N485–N485
33. Uematsu T, Kasami M, Watanabe J. Does the degree of background enhancement in breast MRI affect the detection and staging of breast cancer? Eur Radiol 2011; 21:2261–2267 [PubMed: 21688006]
34. Tofts PS, Brix G, Buckley DL, et al. Estimating kinetic parameters from dynamic contrast-enhanced T1-weighted MRI of a diffusable tracer: standardized quantities and symbols. J Magn Reson Imaging 1999; 10:223–232 [PubMed: 10508281]
35. Essig M, Shiroishi MS, Nguyen TB, et al. Perfusion MRI: the five most frequently asked technical questions. AJR 2013; 200:24–34 [PubMed: 23255738]
36. Yankeelov TE, Luci JJ, Lepage M, et al. Quantitative pharmacokinetic analysis of DCE-MRI data without an arterial input function: a reference region model. Magn Reson Imaging 2005; 23:519–529 [PubMed: 15919597]
37. Fan X, Haney CR, Mustafi D, et al. Use of a reference tissue and blood vessel to measure the arterial input function in DCEMRI. Magn Reson Med 2010; 64:1821–1826 [PubMed: 20665893]
38. Heisen M, Fan X, Buurman J, van Riel NA, Karczmar GS, ter Haar Romeny BM. The use of a reference tissue arterial input function with low-temporal-resolution DCE-MRI data. Phys Med Biol 2010; 55:4871–4883 [PubMed: 20679692]
39. Yang C, Karczmar GS, Medved M, Stadler WM. Estimating the arterial input function using two reference tissues in dynamic contrast-enhanced MRI studies: fundamental concepts and simulations. Magn Reson Med 2004; 52:1110–1117 [PubMed: 15508148]
40. Breast magnetic resonance imaging (MRI) accreditation program requirements. American College of Radiology website. www.acr.org/Quality-Safety/Accreditation/BreastMRI. Revised 2013 Accessed July 15, 2016
41. Preim U, Glaßer S, Preim B, Fischbach F, Ricke J. Computer-aided diagnosis in breast DCE-MRI: quantification of the heterogeneity of breast lesions. Eur J Radiol 2012; 81:1532–1538 [PubMed: 21570225]

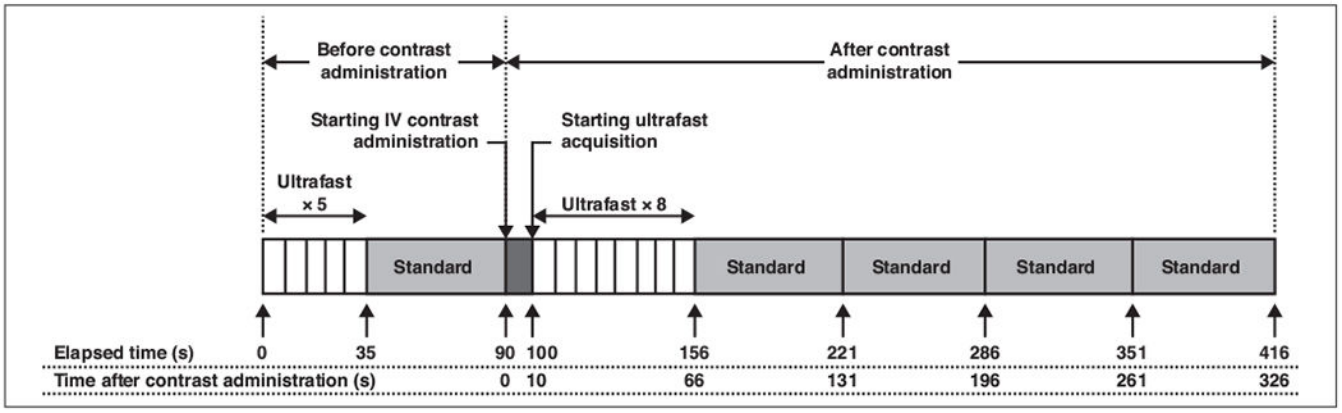

Fig. 1—.

Diagram shows protocols for ultrafast and standard MRI. Ultrafast temporal resolution is 7 seconds; standard, 65 seconds.

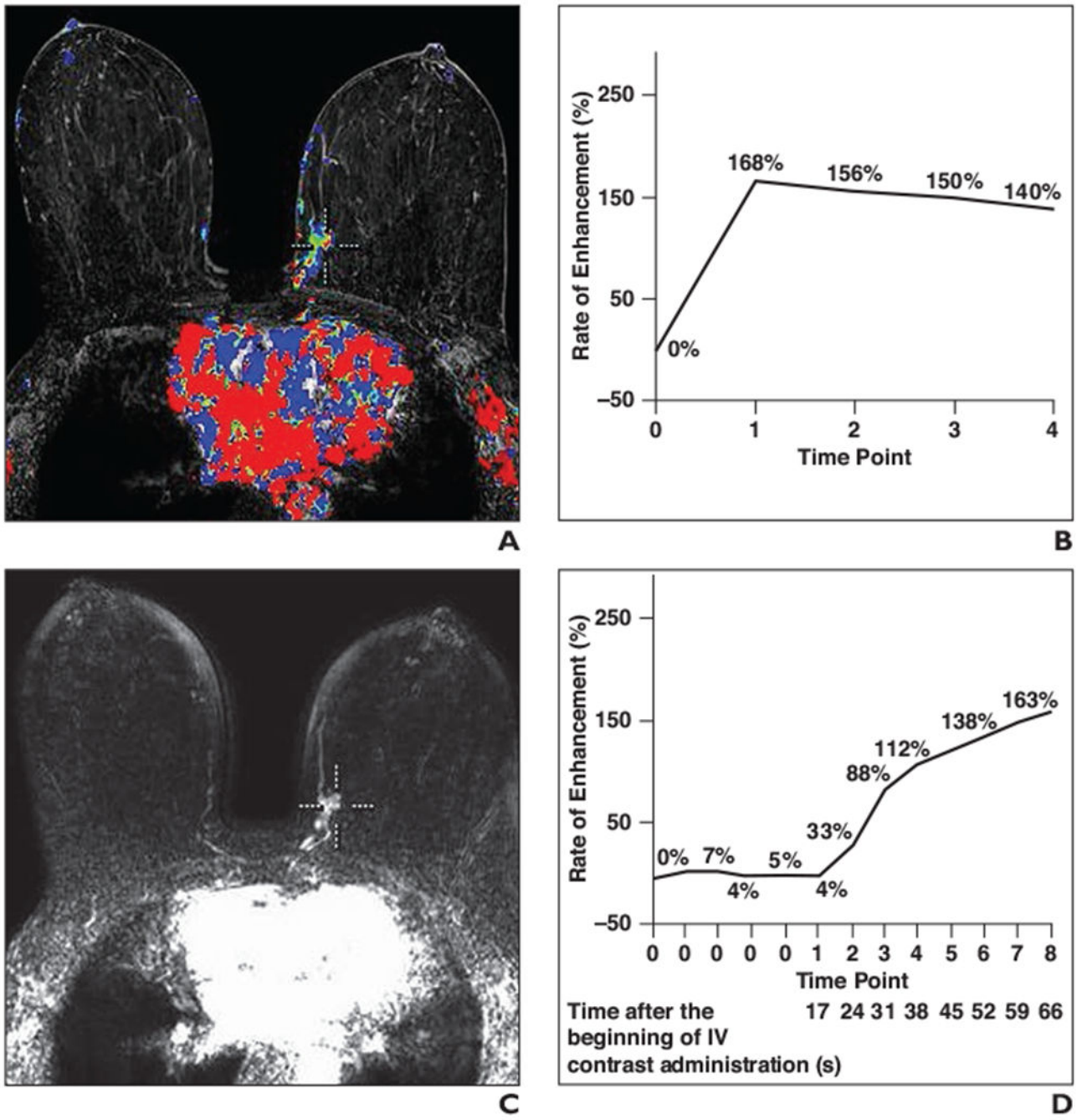

Fig. 2—.

69-year-old woman with grade 3 invasive ductal carcinoma of left breast.

A, Color-coded map of standard MR image shows cursor points at voxel with highest signal intensity in lesion.

B, Graph shows kinetic curve corresponding to **A**.

C, MR image obtained with ultrafast technique shows location of cursor in **A**. In this patient, contrast enhancement in aorta is visible at first time point (C1) on ultrafast image.

D, Graph shows kinetic curve corresponding to **C**.

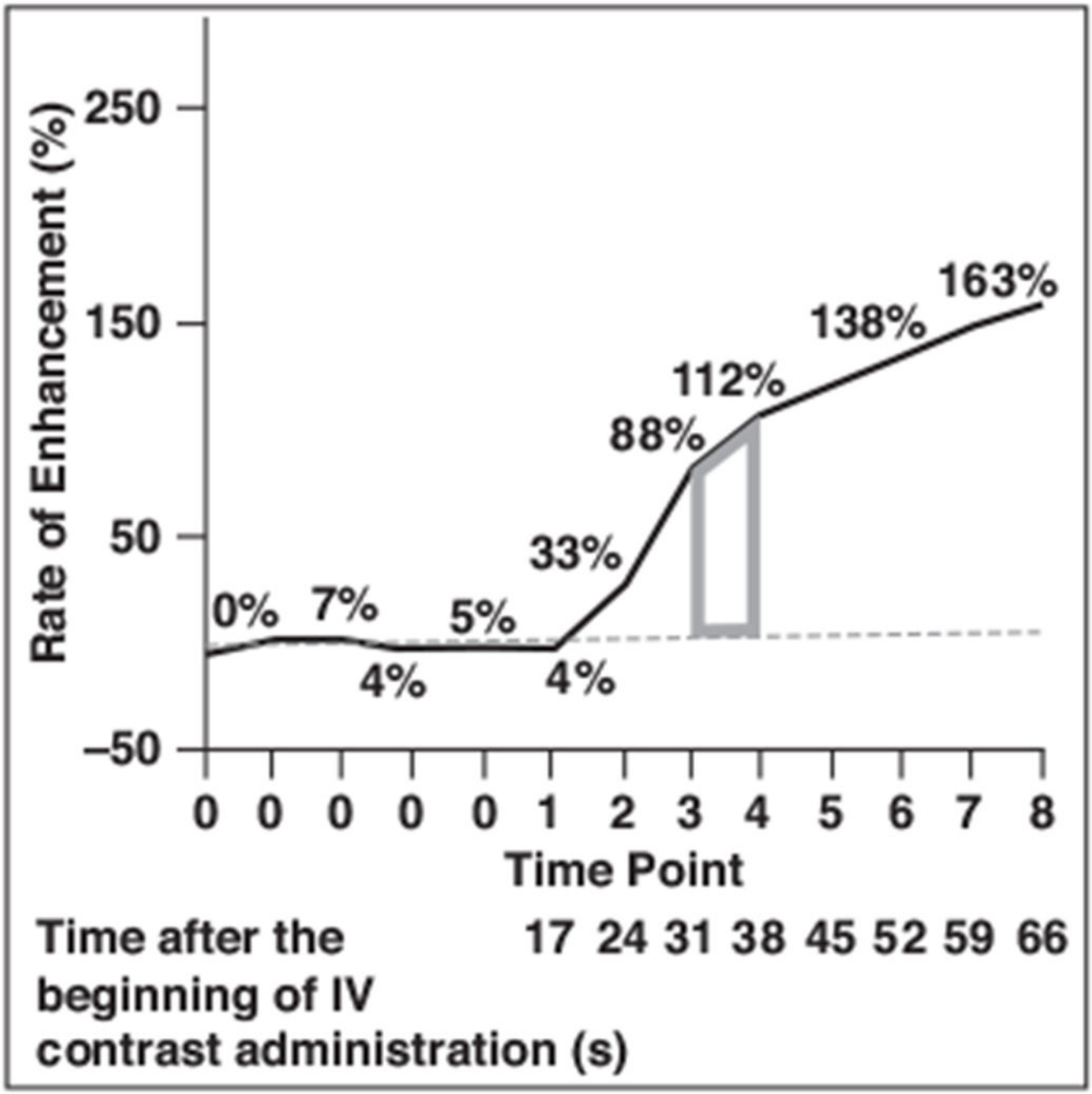

Fig. 3—.

Graph shows kinetic AUC of time point x to time point $x + 1$ as trapezoid (*gray*), which represents AUC of time points 3 and 4. Kinetic AUC for multiple time points can be obtained by addition of each trapezoid from neighboring time points. Dashed line represents $y = 0$.

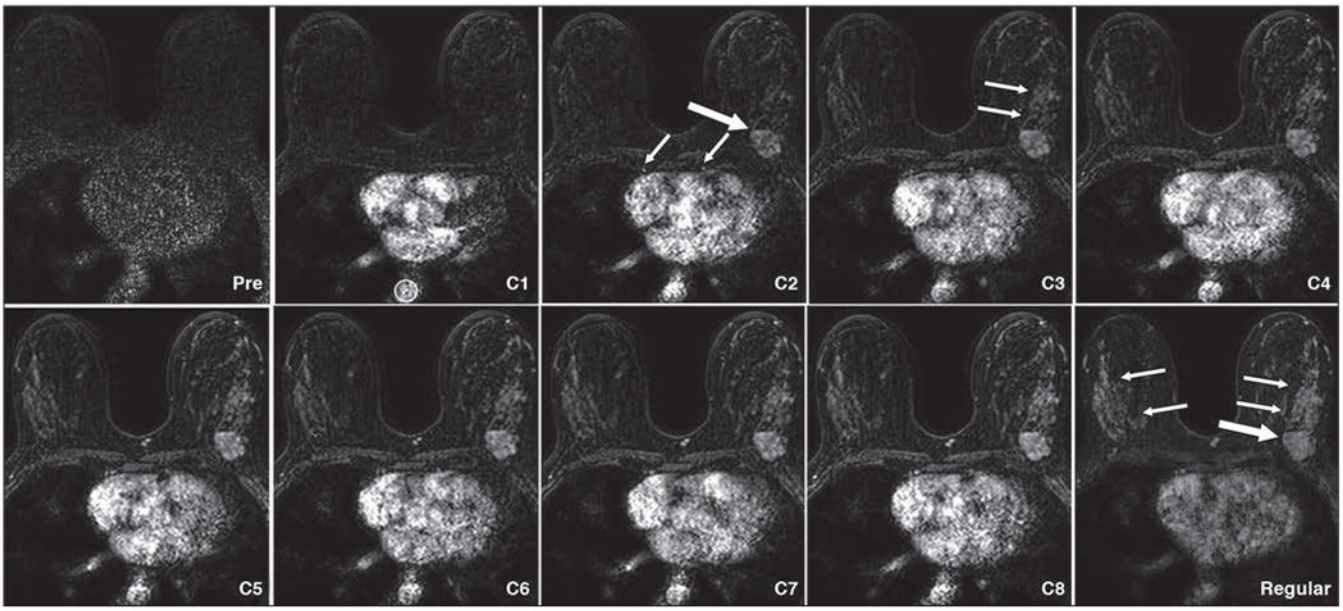

Fig. 4—.

47-year-old woman with metastatic carcinoma of left breast. Series of images from ultrafast acquisition (time points 1–8) and image of same slice on standard (Regular) image (first time point). Image obtained at first time point of ultrafast acquisition (C1) shows R0I (*circle*) on aorta shows more than two times signal intensity of same area on unenhanced image. Therefore, this image becomes C1. On C2 image, malignant tumor (metaplastic carcinoma) becomes visible (*thick arrow*), as do internal mammary arteries (*thin arrows*). C3 image shows background parenchymal enhancement (*arrows*) gradually emerging. Standard image shows degree of background parenchymal enhancement (*thin arrows*) becoming approximately same as signal intensity of tumor (*thick arrow*).

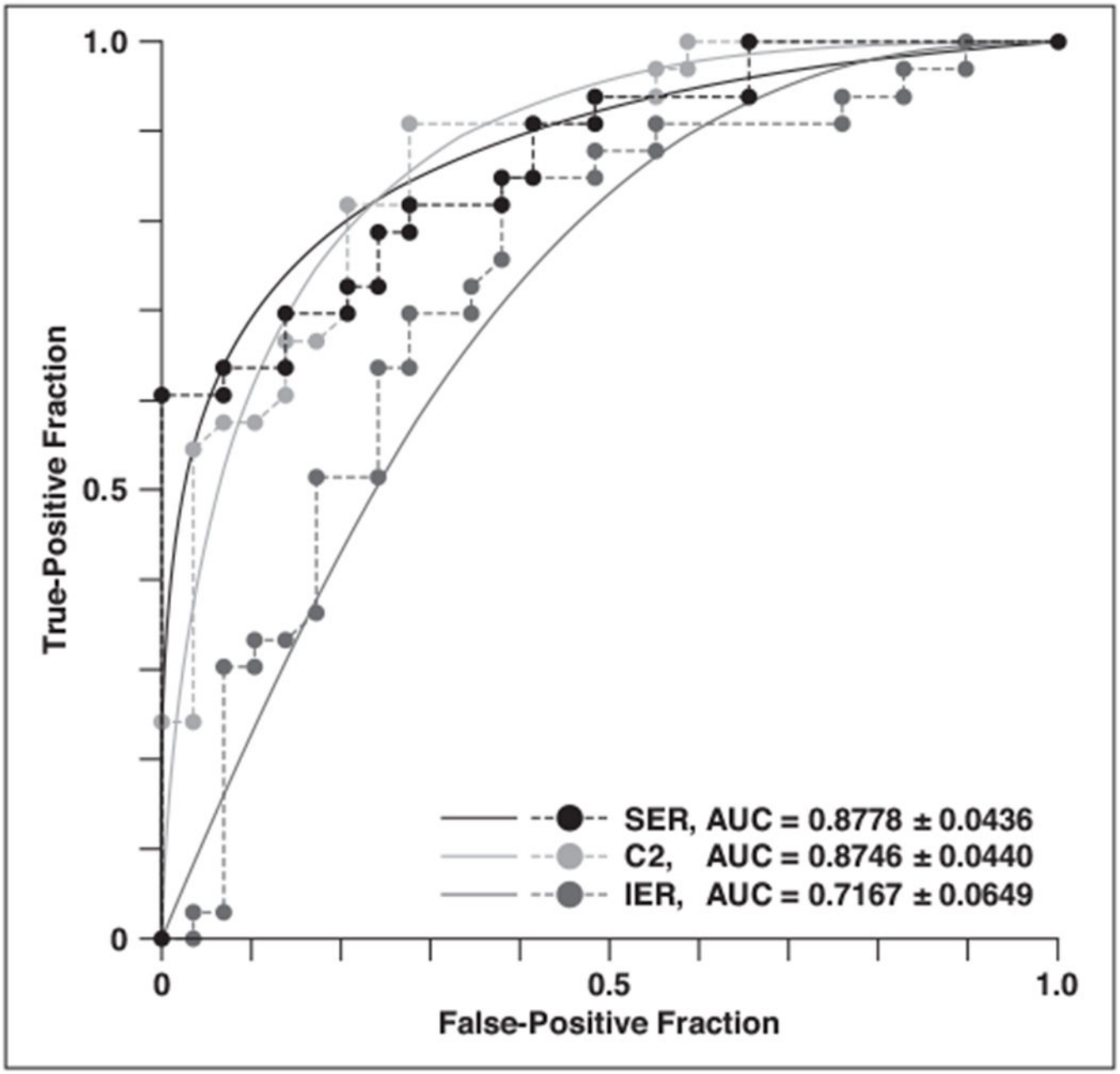

Fig. 5—.

Graph shows ROC curves of enhancement rate at second time point of ultrafast acquisition (C2) and signal enhancement ratio (SER) and initial enhancement rate (IER) of standard image.

TABLE 1:

Patient and Lesion Characteristics

Characteristic	Malignant	Benign	*p*
No.	33	29	
Median age (y)	47 (28–69)	48 (27–69)	0.60
Stage in life			0.61
Premenopausal	17 (52)	17 (59)	
Postmenopausal	16 (48)	12 (41)	
Median lesion diameter (mm)	25 (9–82)	14 (6–97)	<0.0001[a]
Lesion type			0.34
Mass	28 (85)	21 (72)	
Nonmass	5 (15)	8 (28)	

Note—Unless otherwise indicated, values are number of lesions with percentages in percentages. For age and diameter, values in parentheses are ranges.

[a]Statistically significant according to Bonferroni correction of 21 multiple comparisons (critical value, $\alpha = 0.0024$).

TABLE 2:

Acquisition Parameters for Ultrafast and Standard MRI

Parameter	Ultrafast	Standard
TR/TE	3.2/1.6	4.8/2.4
Voxel size (mm^3)	1.5 × 1.5 × 3.0	0.8 × 0.8 × 1.6
SENSE acceleration factor (right-left)	4	2.5
SENSE acceleration factor (foot to head)	2	2
Half scan factor	0.75 (k_y); 0.85 (k_z)	0.85 (k_y); 1 (k_z)
Temporal resolution (s)	7	65
No. of slices	115	215
Flip angle (°)	10	10
FOV (mm)	360	360
Fat suppression method	SPAIR (TR, 155 ms; inversion delay, 80 ms)	SPAIR (TR, 155 ms; inversion delay, 80 ms)

Note—SENSE = sensitivity encoding, SPAIR = spectral attenuated inversion recovery.

AJR Am J Roentgenol. Author manuscript; available in PMC 2019 May 25.

TABLE 3:

Comparison of Initial Enhancement Rate and Signal Enhancement Ratio Between Malignant and Benign Lesions on Standard Images

Value	Malignant	Benign	*p*	AUC[a]	Interclass Correlation Coefficient
Initial enhancement rate	183 ± 45	142 ± 60	0.0014[b]	0.72 ± 0.06	0.88 (0.80, 0.93)
Signal enhancement ratio	1.2 ± 0.2	0.85 ± 0.24	<0.0001[b]	0.88 ± 0.04	0.78 (0.63, 0.87)

Note—Values in parentheses are minimum and maximum.

[a]AUC ± standard error.

[b]Statistically significant according to Bonferroni correction of 21 multiple comparisons (critical value, $\alpha = 0.0024$).

TABLE 4:

Comparison of Enhancement Rate and Kinetic AUC at Each Time Point in the Ultrafast Acquisition

Time Point	Malignant	Benign	*p*	AUC[a]	Interclass Correlation Coefficient
Enhancementrate					
C1	24 ± 35	3.7 ± 4.2	0.0074	0.69 ± 0.07	0.99 (0.98, 1.00)
C2	104 ± 55	34 ± 36	<0.0001[b]	0.87 ± 0.04	0.94 (0.90, 0.97)
C3	152 ± 52	69 ± 54	<0.0001[b]	0.87 ± 0.05	0.96 (0.93, 0.98)
C4	165 ± 54	86 ± 56	<0.0001[b]	0.83 ± 0.05	0.95 (0.92, 0.97)
C5	172 ± 58	99 ± 55	<0.0001[b]	0.81 ± 0.05	0.95 (0.91, 0.97)
C6	174 ± 49	109 ± 57	<0.0001[b]	0.79 ± 0.06	0.93 (0.88, 0.96)
Kinetic AUC					
C1	97 ± 129	21 ± 29	0.0065	0.69 ± 0.07	0.96 (0.94, 0.98)
C2	544 ± 388	151 ± 146	<0.0001[b]	0.88 ± 0.04	0.96 (0.93, 0.97)
C3	1466 ± 698	520 ± 456	<0.0001[b]	0.89 ± 0.04	0.92(0.87, 0.95)
C4	2609 ± 1018	1079 ± 841	<0.0001[b]	0.87 ± 0.04	0.90 (0.84, 0.94)
C5	3825 ± 1373	1746 ± 1235	<0.0001[b]	0.86 ± 0.05	0.88 (0.80, 0.93)
C6	5071 ± 1724	2495 ± 1630	<0.0001[b]	0.85 ± 0.05	0.87 (0.78, 0.92)

Note—Values in parentheses are minimum and maximum.

[a]AUC ± standard error.

[b]Statistically significant according to Bonferroni correction of 21 multiple comparisons (critical value, $\alpha = 0.0024$).